Flat and robust out-of-plane vibrational electret energy harvester

2013 J. Micromech. Microeng. 23 015012

(http://iopscience.iop.org/0960-1317/23/1/015012)

J. Micromech. Microeng. **23** (2013) 015012 (8pp) doi:10.1088/0960-1317/23/1/015012

Flat and robust out-of-plane vibrational electret energy harvester

Yi Chiu and Yen-Chieh Lee

Department of Electrical and Computer Engineering, National Chiao Tung University, Hsin Chu, Taiwan, Republic of China

E-mail: yichiu@mail.nctu.edu.tw

Received 9 August 2012, in final form 21 October 2012
Published 13 December 2012
Online at stacks.iop.org/JMM/23/015012

Abstract
This paper reports the design, fabrication and testing of two types of out-of-plane electret energy harvesters. Copper plates and flexible printed circuit board (FPCB) were used to fabricate the harvesters for a lower fabrication cost and a more robust structure. Several dielectric materials were investigated and SiO_2/Si_3N_4 double layers were found to have better charge stability. The measured surface potential and charge density of the SiO_2/Si_3N_4 electret were -400 V and 13.5 mC m^{-2}, respectively. It was found that charge stability could be improved by multiple corona charging cycles. Using SiO_2/Si_3N_4 as the electret material, the measured power output was 20.7 μW at 110 Hz for 2 G acceleration with a 50 MΩ load for the copper harvester and 0.82 μW at 172 Hz for 2 G acceleration with a 30 MΩ load for the FPCB harvester.

(Some figures may appear in colour only in the online journal)

1. Introduction

Energy harvesting from ambient natural sources, such as vibration and ambient heat, is currently of great interest as self-sustainable power sources for low power CMOS VLSI applications such as wireless sensor networks or personal health monitoring. Among various harvesting approaches, electrostatic vibration-to-electricity conversion is attractive due to its compatibility to IC or MEMS processes and the ubiquity of vibration sources in nature. Electrostatic energy harvesters are capacitive devices and need a bias source to charge the variable capacitor in the harvesters. The bias sources include batteries or voltage supplies [1–4], pre-charged capacitors [5–8], work function difference between two metals [9] and electret [10–22]. Batteries are convenient and inexpensive voltage sources but they have a limited lifetime. Rechargeable batteries can be used to store the harvested energy at the cost of increased system complexity, nonetheless. Work function difference between two metal electrodes is only of the order of 1 V or less. Electret is a dielectric material with a quasi-permanent charge and surface potential of hundreds of volts; therefore, it can be used as a more practical self-sustaining bias source for electrostatic power generation.

Vibrational electret energy harvesters are electrostatic micro power generators with vibration-driven variable capacitors biased by the permanent charge of the electret. The capacitance $C = \varepsilon A/d$ of the variable capacitors can be changed by changing the overlap area A [10–15, 19–21], the gap distance d [16, 17, 19], or the permittivity ε of the dielectric medium between the two electrodes [22]. Electret energy harvesters with varying areas usually employ interdigit electrodes and patterned electret layers that have in-plane motions with respect to each other. The width of the electrode and the electret pattern is usually compatible with the displacement of the moving mass to increase the power output. However, it was reported in [23] that the charge density of the electret decreases with the reducing pattern width. Therefore, it is a less effective approach for small-displacement applications. Electret energy harvesters with varying gaps usually employ cantilever beams with an attached external mass to increase the power output [16]. A micromachined comb structure with the electret material deposited on the electrode sidewalls was also used for a gap-varying electret energy harvester [17]. The cantilever beams or micro machined high-aspect-ratio structures are less robust, especially when they are fabricated in brittle materials, such as silicon. Therefore, we propose in this paper a simpler stacked

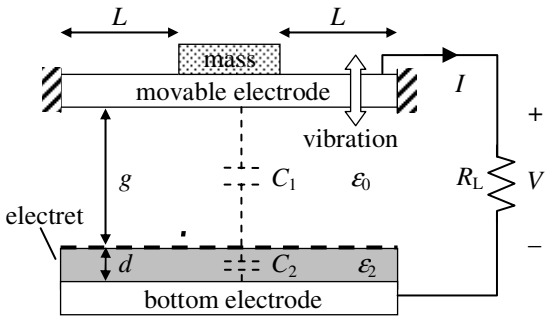

Figure 1. Schematic model of the electret harvester.

structure of ductile or flexible layers for an out-of-plane gap-varying electret harvester to improve the robustness of the device. Since there are no interdigit electrodes or patterns in the device, the fabrication cost can also be reduced. The design, fabrication and testing of the harvesters will be presented.

2. Principles and analysis

The schematic of the gap-varying electret energy harvester and its operation circuit are shown in figure 1. The upper movable electrode forms a parallel-plate capacitor with the bottom electrode on whose surface the electret layer is deposited. Upon the action of the external vibration, the upper electrode moves in the out-of-plane direction, as shown in figure 1, and the gap capacitance C_1 is changed. Since the alignment of the top and bottom parallel electrodes are not critical, they can easily be stacked together with a spacer that defines the gap. To increase the power output, an extra mass made of metal sheets is stacked on the center of the top electrode. The low profile of the extra mass minimizes the total height of the device and maximizes the volumetric power or energy density. The resonant frequency of the mass-spring system can be designed to match the vibration frequency to maximize the power output. The target vibration is at 120 Hz, which can often be found in machinery and household appliances [2]. Nevertheless, the operation and design principles can be applied well to other vibration sources, such as the low-frequency vibration caused by human motion. Two devices based on the schematic in figure 1 are proposed and demonstrated. The copper (Cu) harvester uses copper plates cut from standard copper sheets as the top electrode and the extra mass. The flexible printed circuit board (FPCB) harvester uses commercially available FPCB as the top electrode and a copper plate as the extra mass. The design of the two harvesters is described in the following.

2.1. Cu harvester

The top view and side view of the Cu harvester and its approximate beam length are shown in figure 2. The thin Cu plate is used as the spring and the thick Cu plate is used as the mass. The dimensions and material properties of the plates are shown in table 1. The resonance frequency of the structure is [24]

$$f_0 = \frac{13.86}{2\pi}\sqrt{\frac{EI}{8L^3(M + 0.383M_{\text{beam}})}}, \tag{1}$$

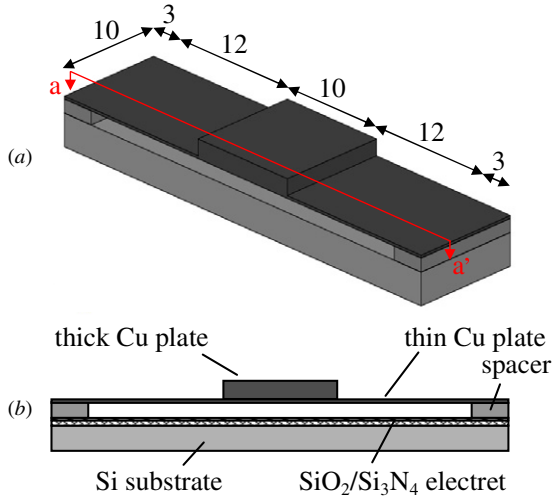

Figure 2. Cu harvester schematics, (*a*) schematic view, (*b*) side view (aa′ cross section). (unit: mm).

Table 1. Dimension and material properties of the movable electrodes.

	Dimension ($L \times W \times H$)	Young's modulus	Density
Thin Cu plate	10 mm × 10 mm × 50 μm	120 GPa	8.9 × 10^3 Kg m^{-3}
Thick Cu plate	40 mm × 10 mm × 300 μm		
FPCB Cu trace	2.4 mm × 200 μm × 17.5 μm		
Polyimide beam (each layer)	2.4 mm × 1000 μm × 25 μm	2.5 GPa	—

where M and M_{beam} are the mass of the shuttle and the beam, respectively, E is the Young modulus of the beam material, $I = WH^3/12$ is the moment of inertia (or second moment of area) of the compliant beam with width W and thickness H and L is the length of the beam, as shown in figure 1. From the parameters in table 1, the bending stiffness of the beam EI is 1.25 × 10^{-5} Nm^2 and thus L can be calculated to be 11.7 mm so that the resonance frequency matches the targeted 120 Hz. The desired length can be achieved by adjusting the position of the spacer.

2.2. FPCB harvester

The top view and side view of the FPCB harvester are shown in figure 3. The FPCB has two layers of polyimide (PI) with patterned Cu traces sandwiched in between. The spring is composed of four fixed-guided thin Cu–PI composite beams, as shown in figure 3(*c*), to reduce the total length of the device as compared to the Cu harvester. The total spring constant of the four composite beams is

$$K_{\text{total}} = 4 \times \frac{12(EI)_{\text{eff}}}{L^3} = \frac{48(EI)_{\text{eff}}}{L^3}, \tag{2}$$

where L is the length and $(EI)_{\text{eff}}$ is the effective bending stiffness of the composite beam given by,

$$(EI)_{\text{eff}} = \sum E_j I_j, \tag{3}$$

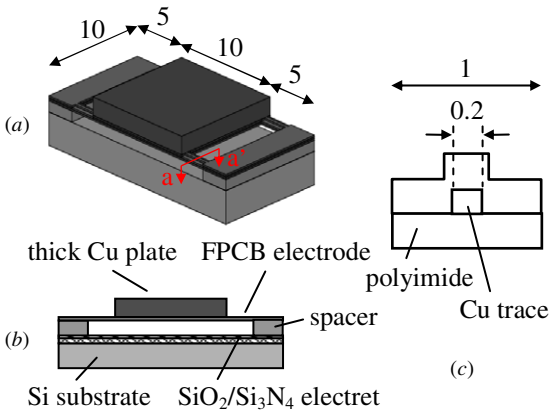

Figure 3. FPCB harvester schematics, (*a*) schematic view, (*b*) side view and (*c*) *aa*′ cross section of the springs. (unit: mm)

where E_j is the Young's modulus, $I_j = W_j H_j^3/12 + W_j H_j \Delta H_j^2$ is the moment of inertia of the jth layer in the composite beam with respect to the neutral axis of the composite and W_j, H_j, ΔH_j are the width, thickness and distance between the centroid of the jth layer and the neutral axis of the composite, respectively. The width of the Cu trace and PI in the composite beam is chosen as 200 and 1000 μm, according to the design rules of the FPCB manufacturer. The calculated effective bending stiffness is $(EI)_{\text{eff}} = 5.38 \times 10^{-8}$ Nm^2, using the material parameters in table 1. By neglecting the mass of the thin Cu–PI beams, the length of the beams can be calculated from the material parameters in table 1 to be 2.4 mm to match the 120 Hz vibration frequency.

The power generation circuit in figure 1 is composed of a bias charge of the surface charge density σ and the total charge Q_t embedded in the electret, a vibration-driven variable capacitor C_1 and an external load R_L. The initial gap distance between the electret and the movable electrode and the thickness of the electret film are g and d, respectively. When the vibration causes a relative displacement of the upper electrode with respect to the lower electrode, the change of capacitance induces a variation of charge on the electrodes and thus leads to an ac current through the external load resistor. The behavior of the harvester is governed by two equations,

$$\begin{cases} -\dfrac{Q_t}{RC_2} + \dfrac{Q_1(t)}{RC(t)} = -\dfrac{\mathrm{d}Q_1(t)}{\mathrm{d}t} \\ m\ddot{x} + b\dot{x} + kx = -m\ddot{y} + F_e. \end{cases}, \tag{4}$$

The first equation is Kirchhoff's circuit law where Q_t is the total charge in the electret and $Q_1(t)$ is the charge on the movable electrode. $C(t)$ is the total capacitance between the movable electrode and the fixed electrode. It is composed of the series connection of two capacitors,

$$\frac{1}{C(t)} = \frac{1}{C_1(t)} + \frac{1}{C_2}, \tag{5}$$

where $C_1(t)$ is the capacitance between the electret layer and the movable electrode and C_2 is the constant capacitance between the electret and the fixed electrode. The second equation is the equation of motion of the proof mass m, where x is the displacement of the mass with respect to the fixed electrode, y is the displacement of the external vibration

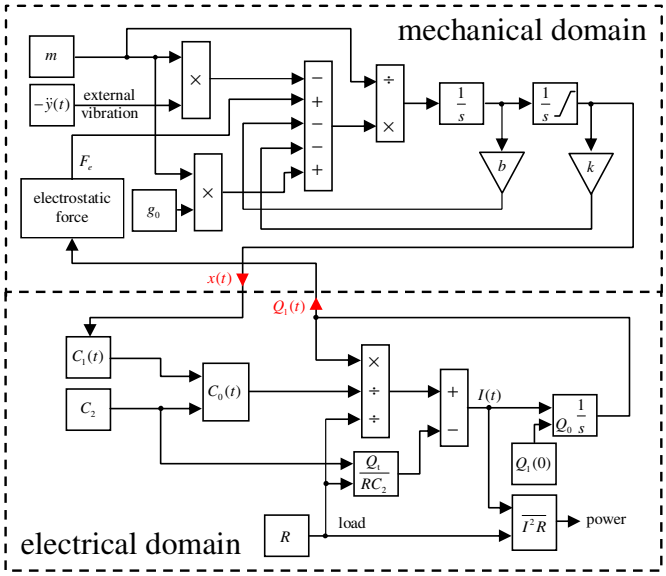

Figure 4. Simulink model.

Table 2. Fixed parameters of the Simulink simulation.

Vibration amplitude	2.45 m s^{-2}
Vibration frequency	120 Hz
Spring constant	203 N m^{-1}
Mass	0.358 g
Quality factor	6.59
Electret and electrode area	10 mm × 10 mm
Electret surface potential	−400 V
Electret thickness	1.05 μm

source, k is the spring constant, b is the mechanical damping constant and F_e is the electrostatic force according to

$$F_e(t) = \frac{Q_1^2(t)}{2\varepsilon_0 A}, \tag{6}$$

where A is the area of the capacitance.

The coupled equations cannot be solved analytically; therefore, the displacement x, charge Q_1 and the output power were calculated by the Simulink simulation shown in figure 4. The electromechanical coupling between the mechanical (x) and electrical (Q_1) domains is through the change of x by the electrostatic force F_e due to Q_1 and the change of Q_1 by the variation of gap capacitance C_1 due to x. Among the numerous design parameters of the harvesters, two were used to optimize the design for maximum output power, i.e. the initial gap g and the external load R_L. The other fixed parameters for an exemplary design are listed in table 2. Figure 5 shows the output power for the initial gap from 100 to 500 μm, and the external load from 20 MΩ to 1.5 GΩ. It shows that the energy harvester can generate a maximum power of 2.02 μW for the load of 660 MΩ when the initial gap is 160 μm. Even though analytical expressions are not available for the output power due to the nonlinear nature of the governing equations, a small-signal model can be derived to describe the characteristics of the figure qualitatively. If the charge $Q_1(t)$ on the movable electrode is written as $Q_1(t) = Q_{10} + \Delta Q_1(t)$, where Q_{10} is the dc bias charge and ΔQ_1(t) is the time-varying component of

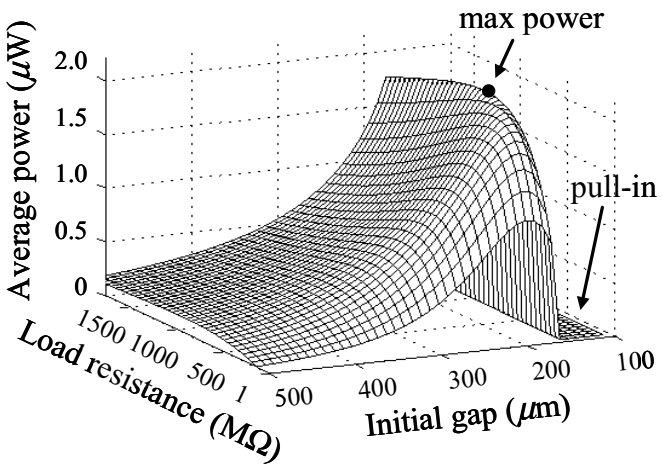

Figure 5. Simulation of average output power for various initial gaps and external loads.

$Q_1(t)$ caused by the vibration, a governing equation of $\Delta Q_1(t)$ can be derived from equation (4),

$$R_L \frac{d\Delta Q_1(t)}{dt} + \frac{\Delta Q_1(t)}{C_0} = E_{10}x, \tag{7}$$

where C_0 and $E_{10} = Q_{10}/\varepsilon_0 A$ are the dc components of the capacitance $C(t)$ and the electric field in the gap, respectively. The equivalent circuit model of equation (7) is a load R_L connected to a vibration-driven voltage source $E_{10}x$ with an output capacitance C_0 and ΔQ_1 is the charge on the capacitance. To maximize the power output delivered to the load in the model, the two impedances, R_L and $1/\omega C_0$, should be matched and they should be minimized. These two trends can be seen in figure 5. Along the load axis, a local maximum can be found for the optimal load that matches the source output capacitance represented by the initial gap distance. Along the gap axis, the power can be increased by reducing the gap (and thus reducing the capacitive impedance). However, the minimum gap for stable operation is limited by the pull-in effect in this electrostatic device. Therefore, the device design parameters for maximum power are close to the pull-in region where the initial gap is less than 150 μm, as shown in figure 5. Even though this device can generate a large amount of power, it only has a small range of operation conditions and fabrication tolerance. Therefore, a more practical device should be designed with less power output to reduce the sensitivity to input and fabrication variations. Since this harvester has a resonating structure, this means that deviations of device dimensions, material properties and input characteristics will cause a discrepancy in the measurement. However, this model can still be used to estimate these tolerances and the non-ideality of the fabricated devices by fitting the parameters with the measured data.

3. Device fabrication and assembly

In recent years, a number of materials have been investigated for electret applications, including CYTOP [13, 15], Teflon AF [11], Parylene HT® [14] and SiO_2 or SiO_2/Si_3N_4 inorganic dielectric materials [12, 25–27]. Double layer SiO_2/Si_3N_4 has the advantage of IC process compatibility and high dielectric

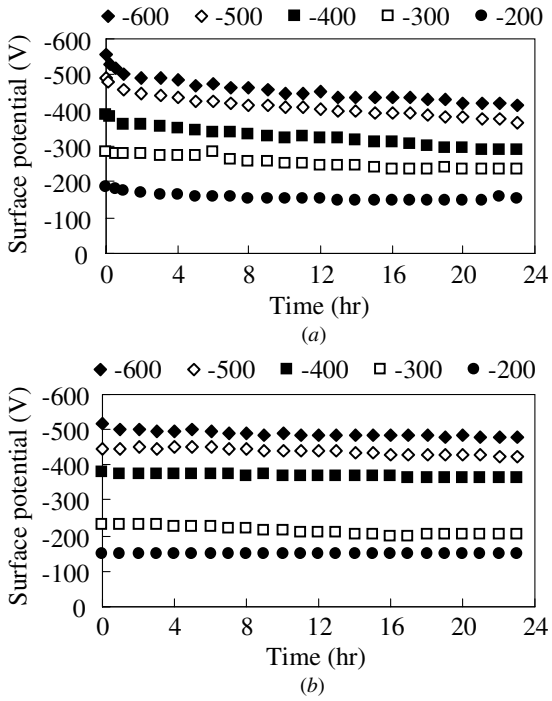

Figure 6. Charge decay after one day for various grid voltages (unit: V) after (*a*) one and (*b*) three charging cycles. The needle voltage was maintained at −4 KV.

strength; its thickness can be accurately controlled by the deposition process. In this research, the SiO_2/Si_3N_4 double layer was charged by corona discharging. The thickness of the oxide and nitride layers were 1 μm and 50 nm, respectively. The corona discharge setup was similar to that in [15, 16]. Negative voltage was applied to the needle electrode and the grid electrode; the back electrode was connected to ground. The sample was placed on a hot plate to maintain specific temperature conditions during charging. The charging experiment was conducted in an atmospheric environment. The gap between the needle tip and the grid electrode was 8 mm; the distance between the grid electrode and back electrode was 4mm. In our experience, a higher needle voltage did not increase the charge density significantly in the SiO_2/Si_3N_4 electret; therefore, the needle voltage was kept between –4 and −5 kV. The samples were prebaked on the hot plate for 30 min at 80 °C and then charged for 30 min at the same temperature. The baking and charging cycles were repeated multiple times to improve the charge stability [28, 29]. The surface potential was measured by an electrostatic voltmeter (Monroe Electronics Model 279). Figure 6 shows the improved short-term charge stability due to the additional charging cycles. Whereas the charge showed more rapid decay from the initial potential corresponding to the grid voltage after the first charging cycle, the charge becomes more stable after three cycles with the average charge retention rate improved from 77% to 94%. This can be explained by the discharge of the shallow charge traps in the dielectric after the first charging cycle and the stabilization of the deeper charge traps after three cycles [29]. Figure 7 shows the long-term charge decay of a sample with three charging cycles at a needle voltage of −4 kV and a grid voltage of −500 V.

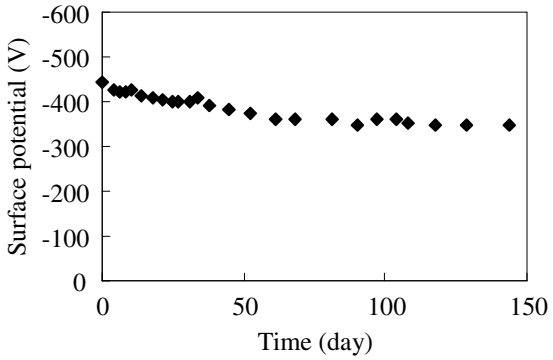

Figure 7. Long term charge stability of SiO_2/Si_3N_4 electret.

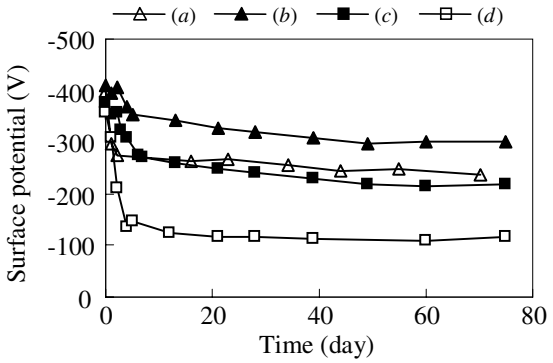

Figure 8. Preliminary charge stability test of PTFE thread seal tapes. The charging conditions (needle voltage/temperature/time) were (*a*) −4 kV/RT/30 min, (*b*) −3.5 kV/RT/30 min, (*c*) −3.5 kV/RT/30 min and (*d*) −3.5 kV/120 °C/10 min. The grid voltage was fixed at −400 V.

For a typical surface potential of −400 V, the corresponding surface charge is $\sigma = \varepsilon_{SiO}\varepsilon_{SiN}V/(\varepsilon_{SiO}d_{SiN} + \varepsilon_{SiN}d_{SiO}) = 13.5\,\mathrm{mC\,m^{-2}}$, where the dielectric constants of silicon oxide and silicon nitride are 3.9 and 7.5, respectively. For a similar length of the measurement time, the charge stability compares well with [19] and [25]. Furthermore, it might be inferred that the charge has reached stabilization since the ratio of the initial potential to the electret thickness is in the same range as in [19]. Other materials were also tested as they had potential as low-cost and flexible electret materials. Figure 8 is the preliminary measurement of the charge stability of thread seal tapes (3M PTFE) under various charging conditions. Acceptable surface potential and charge stability might be achieved under optimized conditions. However, the surface potential was low compared to the SiO_2/Si_3N_4 double layer. Therefore, the double layer was used in the energy harvester in the following experiments.

The device fabrication and assembly process is shown in figure 9. In figure 9(*a*), SiO_2 and Si_3N_4 layers were sequentially deposited on a 4″ silicon wafer by plasma-enhanced chemical vapor deposition. Next in figure 9(*b*), as the spacer of desired thickness, a double-sided tape was bonded onto the silicon wafer. Then the sample was placed in the corona discharging setup to charge the SiO_2/Si_3N_4 double layer. In figure 9(*c*), the top electrode was prepared by stacking two copper plates cut from standard copper sheets, according to the dimensions in table 1, for the copper harvesters. For the FPCB harvesters,

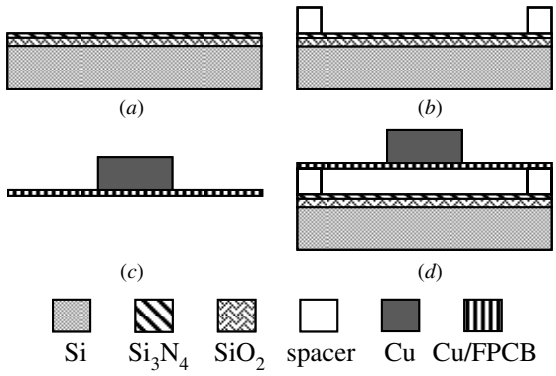

Figure 9. Fabrication and assembly processes.

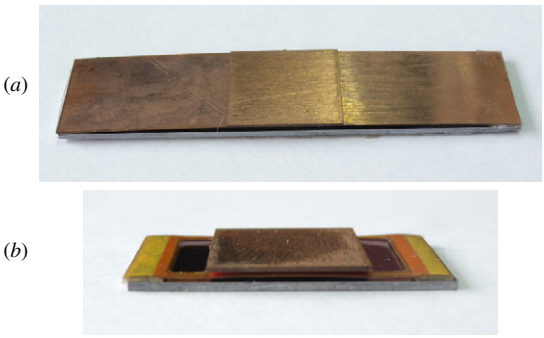

Figure 10. Assembled prototype harvesters, (*a*) Cu harvester and (*b*) FPCB harvester.

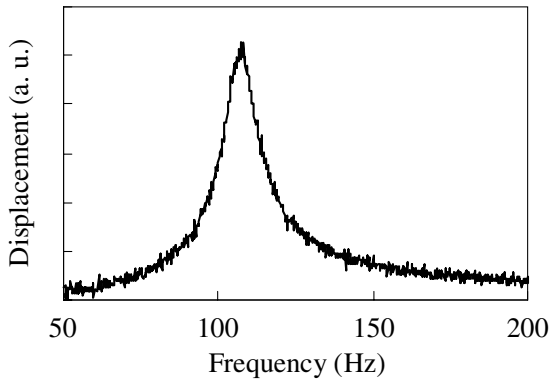

Figure 11. Mechanical frequency response of the Cu harvester.

the 1 × 1 cm^2 thick copper plate was bonded to the FPCB in figure 3. Finally, the top electrode was bonded to the spacer (figure 9(*d*)). Figure 10 shows the fabricated and assembled prototype harvesters. The devices in this study did not have insulation on the metal electrode surface; therefore, the vibration level and electrode displacement must be limited to prevent contact and possible loss of the electret charge. An insulting bump can be fabricated on the surface of the metal electrode or the electret in future studies to prevent a large contact area between the two surfaces in case of a large vibration level or shock.

4. Experiment and discussion

Figure 11 shows the frequency response of the top electrode of a prototype Cu-harvester measured by a laser Doppler

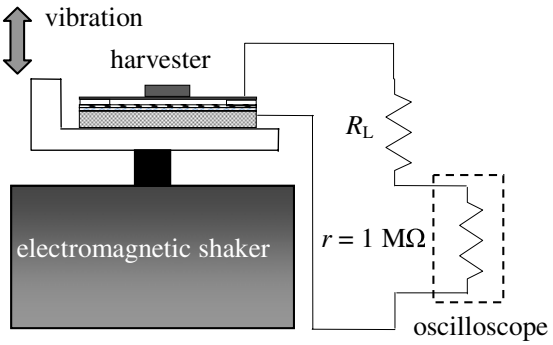

Figure 12. Setup for the power generation experiments.

vibrometer. The resonance frequency is 108 Hz and the quality factor is 9.8 for this device. The difference of the resonance frequency between the measured and expected values are due to the variation of the exact length and mass of the top electrode. The device operation and power generation experiments were conducted using the setup in figure 12. The harvester was fixed on an electromagnetic shaker and tested for different vibration and load conditions. A microscope was used to observe the motion of the electrodes. The amplitude of the relative displacement between the movable and fixed electrodes was estimated to be about 120 μm at 2 G vibration for a harvester with an initial gap of about 360 μm. No pull-in phenomenon was induced at this level of vibration, though it was observed at higher levels of vibration. Since there was no insulation on the top metal electrode, care must be taken to limit the input vibration level and prevent contact between the electrode and the electret. The maximum stress in the metal electrode at 2 G vibration can be calculated to be about 4 MPa, which is much lower than the yield stress 70 MPa of copper. Therefore, the mechanical reliability of the device is ensured.

The output voltage was measured on the small input resistance of the oscilloscope in series with the load resistor R_L. Figure 13(a) shows the output power of a Cu generator as a function of the vibration frequency for a 2 G excitation vibration and 50 MΩ load. The generator has a maximum output power of 20.7 μW at 110 Hz. Figure 13(b) shows the output voltage waveform under the conditions for maximum output power. The measured output power for various excitation levels and load resistance is shown in figure 14, where the power ratio $P_{0.25G}$: P_{1G}: P_{2G} is approximately 1:13:130. According to [30], the maximum power of a linear velocity-damped resonant generator (VDRG) with unconstrained relative displacement x is proportional to the square of the excitation level. Therefore the theoretical power ratio is $P_{0.25G}$: P_{1G}: P_{2G} = 1:16:64. Whereas the power ratio at low-level excitation matches reasonably well with the theory, the power at 2 G is about twice as much as that predicated by the theory. While this phenomenon is being investigated, possible causes include nonlinear electro-mechanical interaction at large amplitudes and a variation of the surface potential/charge during operation.

Figure 14 shows that the maximum power was achieved on a 50 MΩ load, which is quite different from the optimal load of 660 MΩ found in the Simulink simulation in figure 5. The main reason is that the actual harvester is a 1 cm × 4 cm

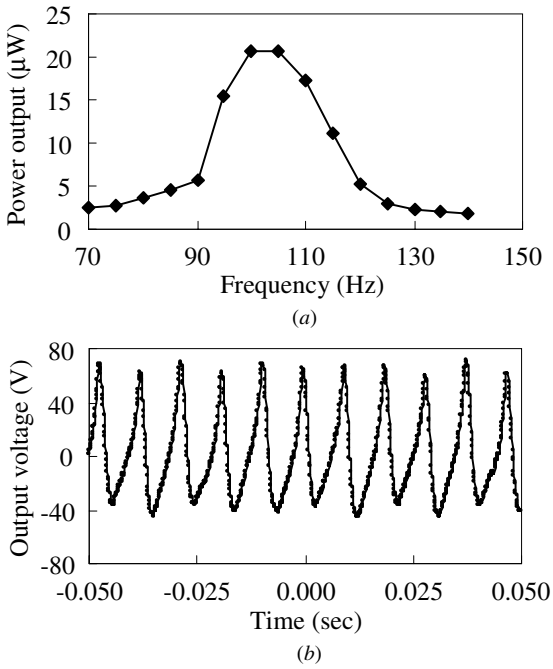

Figure 13. (a) Output power as a function of frequency and (b) output voltage at the maximum power conditions for a 2G vibration and a 50 MΩ load.

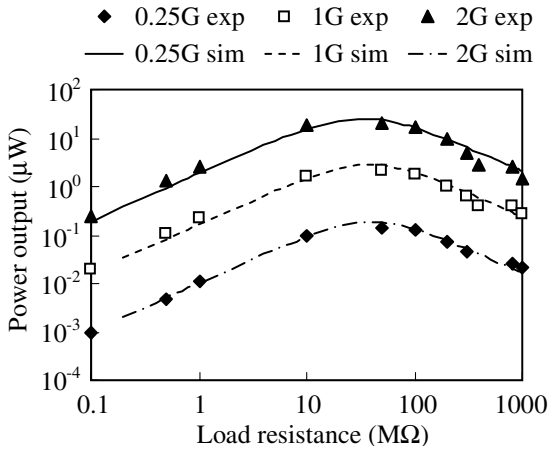

Figure 14. Measured and simulated output power as a function of load resistance. All measurements were made at the constant frequency of 110 Hz. The simulation was obtained with the best parameters fitting the surface potential, initial gap and device capacitance.

capacitor even though the electret area is only 1 cm × 1 cm. Thus there is a parasitic capacitance on the sides of the electret which was not accounted for in the simulation. The other causes of this discrepancy include the variation of the surface potential and initial gap distance due to fabrication errors. By taking the effects of parasitics into account and treating the surface potential and initial gap distance as fitting parameters, a more realistic simulation can be obtained to better match the measured data, as shown in figure 14. Compared to the simulation without parasitics in figure 5, both the maximum power and the optimal load for maximum power were reduced. Since the optimal load without the parasitic capacitance is usually very large (hundreds of MΩ)

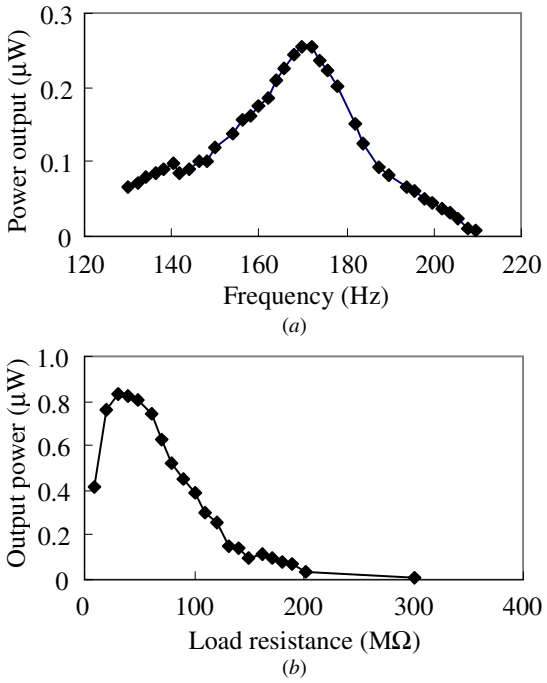

Figure 15. Output power as a function of (*a*) frequency and (*b*) load resistance for a FPCB harvester.

and thus makes the impedance matching to the load difficult, the effect of parasitics may be a solution to a lower and more reasonable optimal load. Further investigation is needed to study the trade-off between the maximum power and the load impedance.

For the FPCB harvester, figure 15(*a*) shows the maximum output power occurs at 172 Hz, which is the resonance frequency of the fabricated device. Figure 15(b) shows the output power as a function of the load resistance. The FPCB harvester can generate a maximum power of 0.82 μW for 2G vibration at 172 Hz on a 30 MΩ load. The difference between the measured and expected (120 Hz) resonance frequencies is due to the additional solder resist layer on the FPCB used to protect the metal traces and prevent solder bridging. The epoxy solder resist layer, which was not considered during the device design, has a thickness of 8–10 μm. From the measured resonance frequency, its Young's modulus can be estimated to be about 7 GPa, consistent with the reported values in the literature [31]. It is also noticed that the output power is relatively small compared to the copper harvester. The possible cause is the decay of the electret charge during the assembly. More experiments are in progress to investigate this issue.

5. Conclusion

This paper presents the design, fabrication and measurement of an out-of-plane electret energy harvester. The optimum values of the initial gap and the load to maximize the output power was found by the Simulink simulation. The experiments showed that the Cu harvester generated a maximum output power of 20.7 μW with a 2 G acceleration at the vibration frequency of 110 Hz for an external load of 50 MΩ. The FPCB harvester generated a maximum output power of 0.82 μW with a 2 G acceleration at the vibration frequency of 172 Hz for an external load of 30 MΩ. The experimental results were different from the simulation due to the difference in the fabrication conditions and device characteristics. Various electret materials were characterized, including SiO_2/Si_3N_4 double layer and PTFE thread seal tapes. The charge stability can be improved by multiple corona charging cycles.

Acknowledgment

This project was supported in part by the National Science Council, Taiwan, R.O.C., under contract nos NSC 99-2220-E-009-027 and NSC-100-2221-E-009-064. The authors are grateful for the use of the facilities at the National Center for High-performance Computing, the National Nano Device Laboratory, the National Chiao Tung Unviersity Nano Facility Center, and the National Tsing Hwa University Center for Nanotechnology, Material Science and Microsystems, Taiwan, R.O.C..

References

[1] Mitcheson P D, Miao P, Stark B H, Yeatman E M, Holmes A S and Green T C 2004 MEMS electrostatic micropower generator for low frequency operation *Sensors Actuators* A **115** 523–9

[2] Chiu Y and Tseng V F G 2008 A capacitive vibration-to-electricity energy converter with integrated mechanical switches *J. Micromech. Microeng.* **18** 104004

[3] Torres E O and Rincón-Mora G A 2009 Electrostatic energy-harvesting and battery-charging CMOS system prototype *IEEE Trans. Circuits Syst. I* **56** 1938–48

[4] Yang B, Lee C, Kotlanka R K, Xie J and Lim S P 2010 A MEMS rotary comb mechanism for harvesting the kinetic energy of planar vibrations *J. Micromech. Microeng.* **20** 065017

[5] Tashiro R, Kabei N, Katayama K, Tsuboi F and Tsuchiya K 2002 Development of an electrostatic generator for a cardiac pacemaker that harnesses the ventricular wall motion *J. Artif. Organs* **5** 239–45

[6] Yen B C and Lang J H 2006 A variable-capacitance vibration-to-electric energy harvester *IEEE Trans. Circuits Syst. I* **53** 288–95

[7] Basset P, Galayko D, Paracha A M, Marty F, Dudka A and Bourouina T 2009 A batch-fabricated and electret-free silicon electrostatic vibration energy harvester *J. Micromech. Microeng.* **19** 115025

[8] Hoffmann D, Folkmer B and Manoli Y 2009 Fabrication, characterization and modelling of electrostatic micro-generators *J. Micromech. Microeng.* **19** 094001

[9] Kuehne I, Frey A, Marinkovic D, Eckstein G and Seidel H 2008 Power MEMS—a capacitive vibration-to-electrical energy converter with built-in voltage *Sensors Actuators* A **142** 263–9

[10] Sterken T, Fiorini P, Altena G, van Hoof C and Puers R 2007 Harvesting energy from vibrations by a micromachined electret generator *Transducers: Proc. 14th Int. Solid-State Sensors, Actuators and Microsystems Conf. (Lyon, France)* pp 129–32

[11] Boland J, Chao Y-H, Suzuki Y and Tai Y-C 2003 Micro electret power generator *MEMS: Proc. 16th IEEE Int. Conf. Micro Electro Mechanical Systems (Kyoto, Japan)* pp 538–41

[12] Naruse Y, Matsubara N, Mabuchi K, Izumi M and Suzuki S 2009 Electrostatic micro power generation from low-frequency vibration such as human motion *J. Micromech. Microeng.* **19** 094002
[13] Suzuki Y, Miki D, Edamoto M and Honzumi M 2010 A MEMS electret generator with electrostatic levitation for vibration-driven energy-harvesting applications *J. Micromech. Microeng.* **20** 104002
[14] Lo H-W and Tai Y-C 2008 Parylene-based electret power generators *J. Micromech. Microeng.* **18** 104006
[15] Sakane Y, Suzuki Y and Kasagi N 2008 The development of high-performance perfluorinated polymer electret film and its application to micro power generation *J. Micromech. Microeng.* **18** 104011
[16] Boisseau S, Despesse G, Ricart T, Defay E and Sylvestre A 2011 Cantilever-based electret energy harvesters *Smart Mater. Struct.* **20** 105013
[17] Yamashita K, Honzumi M, Hagiwara K, Iguchi Y and Suzuki Y 2011 Vibration-driven MEMS energy harvester with vacuum UV-charged vertical electrets *Transducers: Proc. 16th Int. Solid-State Sensors, Actuators and Microsystems Conf. (Beijing, China)* pp 2630–3
[18] Suzuki Y 2011 Recent progress in MEMS electret generator for energy harvesting *IEEJ Trans. Electr. Electron. Eng.* **6** 101–11
[19] Mescheder U, Nimo A, Müller B and Elkeir A S A 2012 Micro harvester using isotropic charging of electrets deposited on vertical sidewalls for conversion of 3D vibrational energy *Microsyst. Technol.* **18** 931–43
[20] Sato N, Ono K, Shimamura T, Kuwabara K, Ugajin M and Sato Y 2012 Analysis of electret-based MEMS vibrational energy harvester with slit-and-slider structure *J. Microelectromech. Syst.* **21** 1218–28
[21] Westby E R and Halvorsen E 2012 Design and modeling of a patterned-electret-based energy harvester for tire pressure monitoring systems *IEEE/ASME Trans. Mechatronics* **17** 995–1005
[22] Boland J S, Messenger J D M, Lo H-W and Tai Y-C 2005 Arrayed liquid rotor electret power generator systems *MEMS: Proc. 18th IEEE Int. Conf. on Micro Electro Mechanical Systems* pp 618–21
[23] Arakawa Y, Suzuki Y and Kasagi N 2004 Micro seismic power generator using electret polymer film *Proc. Power MEMS (Kyoto, Japan)* pp 187–90
[24] Young W C 1989 *Roark's Formulas for Stress and Strain* 6th edn (New York: McGRAW-Hill)
[25] Chen Z, Lv Z and Zhang J 2008 PECVD SiO_2/Si_3N_4double layers electrets on glass substrate *IEEE Trans. Dielectr. Electr. Insul.* **15** 915–19
[26] Mescheder U, Muller B, Baborie S and Urbanovic P 2009 Properties of SiO_2 electret films charged by ion implantation for MEMS-based energy harvesting systems *J. Micromech. Microeng.* **19** 094003
[27] Leonov V and van Schaijk R 2010 Patterning of inorganic electrets *IEEE Trans. Dielectr. Electr. Insul.* **17** 994–1000
[28] Sessler G M 1980 *Electrets* (Berlin: Springer)
[29] Sprenkels A J, Olthuis W and Berveld P 1988 The application of silicon dioxide as an electret material *ISE: Proc. 6th Int. Symp. on Electrets* pp 165–69
[30] Mitcheson P D, Green T C, Yeatman E M and Holmes A S 2004 Architectures for vibration-driven micropower generators *J. Microelectromech. Syst.* **13** 429–40
[31] Wouters K and Puers R 2009 Determining the young's modulus and creep effects in three different photo definable epoxies for MEMS applications *Sensors Actuators* A **156** 196–200